SYNTHESIS AND INFLUENCE OF Al_2O_3 NANOPARTICLES ADDITION ON THE STRUCTURAL AND MICROSTRUCTURE PROPERTIES OF $YBa_2Cu_3O_7$ CERAMIC SUPERCONDUCTORS

by

YASMIN BINTI ABDUL KARIM

A report submitted in fulfillment of the requirements for the degree of Bachelor of Applied Science (Materials Technology) with Honours

FACULTY OF EARTH SCIENCE
UNIVERSITI MALAYSIA KELANTAN

2017

ACKNOWLEDGEMENTS

In the name of Allah, the Most Gracious and the Most Merciful

Alhamdulillah, all praises to Allah for the strengths and His blessing in completing this thesis. Special appreciation goes to my supervisor, Dr Arlina Binti Ali, for her supervision and constant support. Her invaluable help of constructive comments and suggestions throughout the experimental and thesis works have contributed to the success of this research. Not forgotten, my appreciation to my co-supervisor, Prof Dr Julie Juliewatty for her support and knowledge. My acknowledgement also goes to all the technicians and office staffs of the Material Science Laboratory for their cooperations. Sincere thanks to all my friends especially Adibah, Rozi, Iskandar and others for their kindness and moral support during my study. Thanks for the friendship and memories. Last but not least, my deepest gratitude goes to my beloved parents, Mr. Karim Bin Hassan, Mrs. Samsiah Binti Seraj and also to my elder sister, Yana for their endless love, prayers and encouragement. To those who indirectly contributed in this research, your kindness means a lot to me. Thank you very much.

Synthesis and Influence of Al_2O_3 Nanoparticles Addition on the Structural and Microstructure Properties of $YBa_2Cu_3O_7$ Ceramic Superconductors

ABSTRACT

Superconductivity is a phenomenon in which a number of pure metals and alloys offer no resistance to the passage of electrical current below a certain critical temperature. Throughout the past research on the superconductivity, High Temperature Superconductor (HTSC) such as $YBa_2Cu_3O_7$ was being focussed for their properties as a type-II superconductor. However, this research was conducted by introducing the addition of Al_2O_3 nanoparticles in order to enhance its properties. The aim of this research is to synthesize $YBa_2Cu_3O_7$ pure powder by solid state reaction method. Besides, this research is also focussed in examine the influence of Al_2O_3 nanoparticles addition on $YBa_2Cu_3O_7$ ceramic superconductors. Finally, this study intended to identify the effects of Al_2O_3 nanoparticles addition on the crystal structure and microstructure of $YBa_2Cu_3O_7$. The XRD result of the Al_2O_3 nanoparticles addition indicate that all sample can be indexed to Y-123 phase by the dominant peak of (103) and (013) with the increment of *a* and *c* lattice parameter. The increment length of lattice parameter indicating the Al^{3+} ions occupy in both Y and Cu sites. Furthermore, the addition of Al_2O_3 nanoparticles does reduce the orthohombicity of sample. The crystallite size of sample was 28.14 nm at 0.50 wt% of addition. The TGA prove that the sample produce a complete stabilize final product at 900 to 950^oC.

Synthesis and Influence of Al_2O_3 Nanoparticles Addition on the Structural and Microstructure Properties of $YBa_2Cu_3O_7$ Ceramic Superconductors

ABSTRAK

Superkonduksian adalah satu fenomena di mana beberapa logam tulen dan aloi menawarkan tiada rintangan kepada peredaran arus elektrik di bawah suhu kritikal tertentu. Sepanjang kajian mengenai kesuperkonduksian, Suhu tinggi Superkonduktor (HTSC) seperti $YBa_2Cu_3O_7$ diberi tumpuan untuk sifatnya sebagai superkonduktor jenis-II. Walau bagaimanapun, kajian ini telah dijalankan dengan memperkenalkan penambahan nanopartikel Al_2O_3 untuk meningkatkan sifat kesuperkonduksiannya. Tujuan kajian ini adalah untuk mensintesis $YBa_2Cu_3O_7$ serbuk tulen dengan kaedah tindak balas keadaan pepejal. Selain itu, kajian ini juga memberi tumpuan dalam mengkaji pengaruh Al_2O_3 nanopartikel pada superkonduktor seramik $YBa_2Cu_3O_7$. Akhir sekali, kajian ini bertujuan untuk mengenal pasti kesan-kesan Al_2O_3 nanopartikel tambahan kepada struktur kristal dan mikrostruktur $YBa_2Cu_3O_7$. Sintesis YBCO telah berjaya daripada langkah proses pengkalsinan dan pensinteran. Hasil XRD dengan penambahan Al_2O_3 nanopartikel menunjukkan bahawa semua sampel boleh diindeks kepada Y-123 fasa oleh puncak yang dominan pada (103) dan (013) dengan peningkatan parameter *c* dan *a* kekisi. Panjang kenaikan parameter kekisi menunjukkan ion Al^{3+} menduduki dalam kedua-dua Y dan Cu tapak. Tambahan pula, penambahan nanopartikel Al_2O_3 mengurangkan ortorombik sampel. Saiz kristal sampel adalah 28.14 nm pada 0.50% berat penambahan Al_2O_3 nanopartikel. Hasil analisis TGA membuktikan bahawa sampel produk terakhir yang stabil terhasilkan pada suhu 900 kepada 950^oC.

DECLARATION

I declare that this thesis entitled "Synthesis and Influence of Al_2O_3 Nanoparticles Addition on the Structural and Microstructure Properties of $YBa_2Cu_3O_7$ Ceramic Superconductors" is the result of my own research except as cited in the references. The thesis has not been accepted for any degree and is not concurrently submitted in candidature of any other degree.

Signature : _____

Name : YASMIN BINTI ABDUL KARIM

Date : 31 December 2016

TABLE OF CONTENT

LIST OF TABLES

LIST OF FIGURES

LIST OF SYMBOLS AND ABBREVIATION

a, b, c	Lattice parameter
T_c	Superconductor transition temperature
J_c	Critical current density
HTSC	High Temperature Superconductor Ceramic
wt%	Weight percentage
Y-211	$YBa_2Cu_3O_5$
Y-123	$YBa_2Cu_3O_7$
YBCO	$YBa_2Cu_3O_7$
XRD	X-ray diffraction
TGA	Thermogravimetric Analysis
K	Kelvin
Å	Angstrom
D	Debye scherrer
Δ	Energy gap

CHAPTER 1

INTRODUCTION

1.1 Background of Study

Superconductivity is a phenomenon of the electric resistivity of a certain material decreases to zero in certain temperature. The resistivity of a metal decrease when the temperature is below to a certain point (Lleonart, 2014). In 1911, the Dutch physicist, Heike Kamerlingh Onnes cooled mercury down to the boiling temperature of liquid helium (4.2 K). Thus, the phenomenon that explains this sudden change in the electrical properties of superconductor materials is due to the Cooper pair formation. Yttrium barium copper oxide (YBCO) is a superconducting material with a phase transition at 92 K that is above the boiling point of liquid nitrogen (Aparimita, 2011). Besides, YBCO remains the best studied for ceramic superconductors (Alecu, 2004). It has an orthorhombic geometry that gives the ability as superconductor materials. The YBCO have in common the presence of copper oxide layers, with superconductivity taking place between these layers. CuO_2 layer is the basic feature of all high temperature superconductor (HTS) with transition temperature greater than 40 K (Howe, 2014).

1.1.1 History of Superconductor

The industrial developments and research for superconductive devices are relatively decreases due to the cost and reliability of refrigeration needed to cool materials into superconductive states (Thakur & Chawla, 2015). However, the new discovery of high critical temperature superconductor led to rapid succession in the industry. Besides, the new scientific discovery by the researchers must strive to explain their theories in order to contribute to the theory of superconductor. The table 1.1 shows the discoveries and development in superconductivity study area.

Table 1.1 : The discoveries and development in superconductivity area (Sheahen, 2004).

Researcher	Discovery	Year
Kammerligh Heiki Onnes	Resistance of mercury at 4.2 K	1911
Meissner & Oshsenfeld	Meissner Effect Principle	1933
Gorter & Casimir	Two Fluid Model	1934
Gizburg & Landau	Phenomenological Theory	1950
Bardeen, Cooper & Schrieffer	BCS Theory	1957
Abrikosov	Existence of Type-I and Type-II Superconductor	1957
Brian Josephson	Josephson Effect	1962
Bednorz & Muller	La-Ba-Cu-O at 35 K	1986
Wu and Chu	$YBa_2Cu_30_7$ at 90 K	1987

1.2 Problem Statement

For the past decade, it is a great deal of a research that is usually being concerned on the efficiencies of power production and its improvement of power quality which become priorities in the industry (Thakur & Chawla, 2015). An important fraction of the research on High-Temperature Superconductor Ceramic (HTSC) was devoted to explicate their structure. The HTSC such as $YBa_2Cu_3O_7$ (YBCO) is extensively being improved in order to create a better quality in term of its structural and microstructure. However, synthesizing a superconducting material with a transition temperature close to room temperature is a major challenge (Aparimita, 2011). Heading towards the current, the research and development of superconductors were focus by the addition of a metallic element that will enhance the performance of ceramic superconductivity. Various attempts have been made to tune the properties of superconducting materials in the recent past. The addition of Al_20_3 nanoparticles could creates the possibility of the enhancement in YBCO as a ceramic superconductor. Despite from being excellent superconductors, the addition of a metallic element of Al_20_3 nanoparticles to YBCO could produce a better quality of the superconductor in term of its structural and morphology. On top of that, YBCO with the addition of Al_20_3 nanoparticles could prove to be potential candidates for superconducting applications.

1.3 Objectives

The objectives of this research are:

I. To synthesize $YBa_2Cu_3O_7$ by solid state reaction method.

II. To study the influence of Al_2O_3 nanoparticles addition on $YBa_2Cu_3O_7$ superconductors with different weight percentages (x= 0.00 – 3.50 wt%).

III. To identify the effects of Al_2O_3 nanoparticles on the crystal structure and microstructure of $YBa_2Cu_3O_7$.

1.4 Expected Outcome

This research study focuses on the influence of Al_2O_3 nanoparticles addition on the structural and microstructure of the superconductor. It covers the process of $YBa_2Cu_3O_7$ synthesis by solid state reaction and the effect of Al_2O_3 nanoparticles addition with difference weight percentages (wt%). The pure $YBa_2Cu_3O_7$ is an orthorhombic crystal structure confirmed by XRD analysis (Aparimita, 2011). Besides, the addition of Ag is expected to have significant changes in term of the crystal structure, where the planes or the axis orientation will cause any changes in term of their lattice parameter. In spite of the fact that Cu and Ag are from the same group of the periodic table of elements, Ag substitutes for Cu in the YBCO superconductors (Zhang *et al.*, 1995). Thus, the effect of Ag respect to Cu atom will produce a compound that has the variation of the lattice parameter *(a, b, c)* (Widad *et al*., 2013).

For the morphology, the excess metallic Ag will fill the pores of the bulks and encouraged the formation of larger stacks of flat rectangular platelets, resulting in a *c*-axis preferred orientation (Salamati *et al*, 2001). Generally, it is observed from the literature reviews that the addition of Ag in HTSC improves the inter-grain connectivity due to the weak-links and superconductivity parameters (Jabbar *et al*., 2014). Furthermore, it reduces the grain size and the increase of metallicity across the grain boundaries (Parida, 2011).

CHAPTER 2

LITERATURE REVIEW

2.1 Superconductivity of $YBa_2Cu_3O_7$

Superconductivity is a property of metal, alloys, nor chemical compound at transition temperature or temperature called as the critical temperature where resistivity disappear and they becomes a perfect diamagnetic in nature due to the Meissner effect (Parida, 2011). Superconductivity is a phenomenon whereby a number of pure metals and alloys offer no resistance to the passage of electrical current below a certain critical temperature (Lundy *et al*., 1989). The structural, transport and magnetic properties are responsible for the superconductivity behaviour of $YBa_2Cu_3O_7$ (Grant *et al.,* 1987). Bulk $YBa_2Cu_3O_7$ superconductors have been widely investigated, as the material show great potential in several engineering applications (Devendra *et al.,* 2013).

2.2 Meissner Effect

The superconductor is the material which has zero magnetic field and flux is known as to be in the Meissner state. Meissner and Ochsenfeld measured magnetic flux arrangement outside superconducting specimens which has been cooled below their transition temperature while in a magnetic field. This phenomenon is also known as perfectly diamagnetic (Aparimita, 2011). As for $YBa_2Cu_3O_{7,}$ the research for levitation properties and magnetisms is reveal by placing the superconductor in liquid nitrogen (77K) with a small magnet which is placed above the sample. This phenomenon creates the mutual repulsion that lead to the levitation of magnet (Owens & Poole, 2002). The levitation phenomenon of magnet over superconductor sample is shows in figure 2.1.

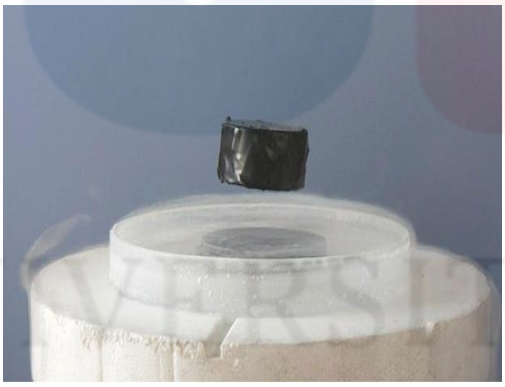

Figure 2.1 : Levitation image of a magnet over superconductor sample (Howe, 2014)

2.3 Types of Superconductors

2.3.1 Type-I Superconductor

The superconducting materials which exhibit the total expulsion of flux (Meissner effect) up to a critical magnetic field Hc(0) and penetrate the material will behave as a normal conductor. This type of superconductors are called type-I superconductor. The examples of Type-I superconductors samples are Pb, Hg and Sn. These superconductors are also known as soft normal superconductors (Prozorof *et al.,* 2008). The magnetic phase diagram for type-I superconductors is show in the figure 2.2 as below.

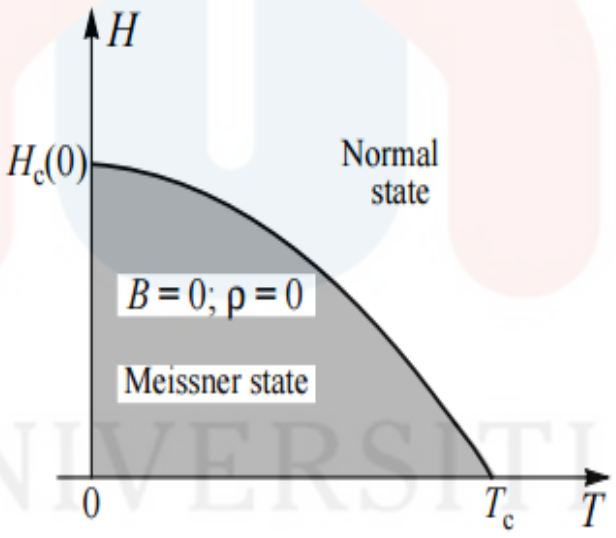

Figure 2.2 : Magnetic phase diagram for type–I superconductors (one critical field Hc(0) exists) (Mourachike, 2004)

2.3.2 Type-II Superconductor

In type II superconductors, the Meissner effect occurs only as long as the applied magnetic field stays below a certain critical field (Hc_1). At higher fields, the magnetic flux starts penetrating into the material and the superconductor enters the mixed state. As an upper critical field (Hc_2) is reached, the material becomes normal and superconductivity is lost (Lleonart, 2014). YBCO is a high-temperature superconductor which obeys the properties of type II superconductors. It is known as hard superconductors that can bear high magnetic field (Aparimita, 2011). The figure 2.3 below shows the magnetic phase diagram for type-II superconductors.

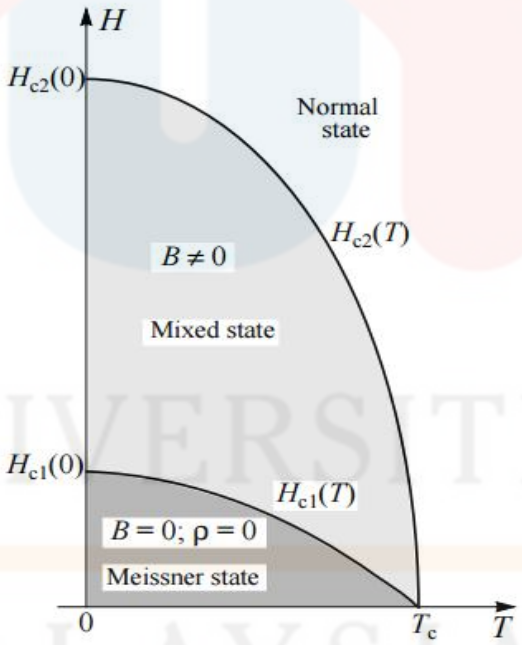

Figure 2.3 : Magnetic phase diagram for type-II superconductors (exist lower critical field, Hc_1 & upper critical field, Hc_2) (Mourachike, 2004)

2.4 Ceramic Oxide Superconductor

Ceramic materials are inorganic or non-metallic materials which may be crystalline or partly crystalline. Ceramic are formed by thermal action of heating and subsequent cooling. Besides, it is brittle, hard and strong in compression. They are weak in shearing and tension, but able to withstand chemical erosion which occurs in caustic or acidic environment. Generally, ceramics material can withstand very high temperatures in range of 1000˚C to 1600˚C (Vinila *et al.,* 2014). Furthermore, ceramics describes an engineering activity which embracing the development of ceramic component and produce a significant advance in electroceramics (Moulson & Herbert, 2013). In 1986, a new class of ceramic material superconductors discovered by Swiss and German scientists which made from rare earth elements such as lanthanum and yttrium mixed with copper oxides (Felt & Nowotny , 1992).

2.5 Copper Oxide-based High Temperature Superconductor

The copper oxide-based high-temperature superconductor is first discovered by Bednorz and Muller in 1986 and is perhaps the most popular and most studied of all classes of superconductor. Some of the common systems of HTS are shows in table 1.1. The CuO_2 plane within the structure are believed to be strongly associated with the superconductor properties. One remarkable property of HTS is the short coherence length (3 - 20Å) which is several orders of magnitude shorter than that of the convectional superconductor. Recalling the Coulomb repulsion force, F between two like chargers is inversely proportional to distance, r square $F \propto \frac{1}{r2}$. This indicate

that the Coulomb repulsion is much higher for Cooper pairs in HTS compared to a conventional superconductor. As such, the pairing system in HTS must provide a pairing energy that is several orders of magnitude larger than that of convectional superconductor in order to overcome this strong Coulomb repulsion (Shukor, 2009).

2.6 BSC Theory

BCS theory is formulated by Bardeen, Cooper and Schrieffer in 1957 which known as the microscopic theory of superconductivity. BCS theory is the interaction of a "gas" in conducting electrons by the elastic waves of the crystal lattice or phonon (Mourachike, 2004). According to Cyrot and Pavuna, 1992, it is also known to have the ability of electron to travel easily, where there is no loss in current due to the zero resistant in electricity transfer. Thus, two electrons in a vacuum will repel each other, but in a form the electron pairing. These electrons couple to the lattice resulting in pairs, called Cooper pairs (Tahirbegi, 2014). The electron pairing or Cooper pairs are form by the interaction of electron phonon (Mourachkine, 2002). Thus, the cooper pairs as a superconductor is heated by thermal agitation. An amount of energy or energy gap (Δ) is used to break down the pairs. The energy supplied to the superconductor must be at least twice as great (2Δ) in order to break and separate the pair (Rose-Innes & Rhoderick, 1928). In addition to electron pairing, superconductivity requires long-range phase coherence which is cause by the overlap of their wave functions (the wave-function coupling) among the Cooper pairs.

2.7 $YBa_2Cu_3O_7$ Crystal Structure

The structure of YBCO plays an important role in superconductivity behaviour (Safranski, 2010). The crystal structure of $YBa_2Cu_3O_7$ or "Y123" is layered and characterized by copper-oxygen plane and copper-oxygen chains. It has been shown by several groups of scientists that the new HTS are structurally members of a crystallographic family known as perovskites (Hazen *et al.*, 1987). The YBCO layer has a stacking sequence along the *c*-axis which formed into CuO–BaO–CuO2–Y–CuO2–BaO. It consists of $BaCuO_3$ and $YCuO_3$ in stacked cubes which being separated by planes of CuO_2 and yttrium atoms between the copper-oxygen planes.

It is referred to a complex layer of metal oxide. Thus, the planes consist of a square lattice of copper atoms connected by an oxygen atom. In the unit cell of $YBa_2Cu_3O_7$, the chain of CuO are exactly parallel to the copper-oxygen planes, where barium atom was situated between them (Howe, 2014). Superconductivity in YBCO triple cubes structure resides in the Cu-O planes (Sahoo & Behera, 2012). The fully oxidized compound of $YBa_2Cu_3O_7$ which based on the structure on the perovskite structure which has an orthorhombic as the coordination of geometry for a unit cell, where the lattice parameter, a = 3.82 Å, b =3.89 Å, c =11.68 Å along (100), (010) and (001) direction (Benzia *et al*, 2004). Thus, figure 2.4 shows the crystal structure of $YBa_2Cu_3O_7$, while the information for its lattice parameter is detailed in table 2.1 as below.

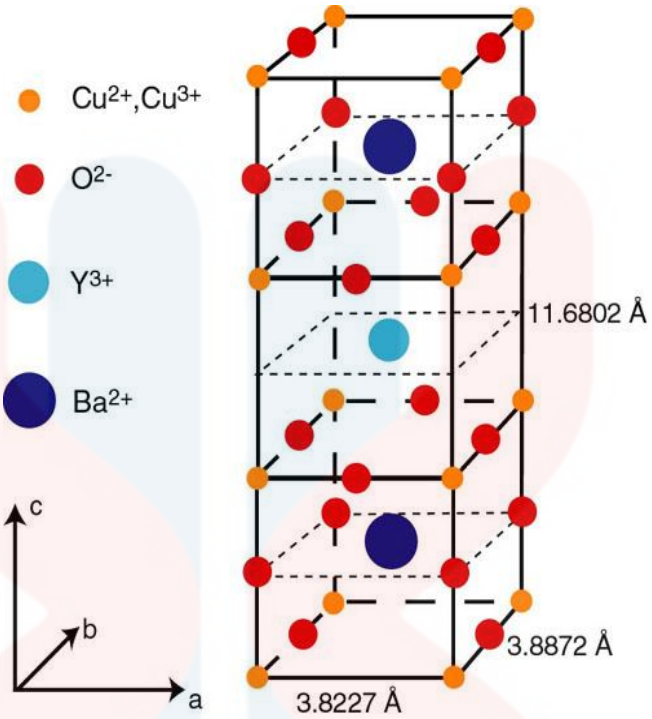

Figure 2.4. The crystal structure of a single unit cell of $YBa_2Cu_3O_7$ (Aparimita, 2011)

Table 2.1 : The lattice parameter of $YBa_2Cu_3O_7$.

Lattice Parameter	Direction	Å
a-axis	100	3.82
b-axis	010	3.89
c-axis	001	11.68

2.8 Addition of Silver (Ag)

Ag is known as a metallic with the atomic number of 47. It is a transition metal with high electrical conductivity and thermal conductivity. The metal additive such as Ag with $YBa_2Cu_3O_7$ will form into a ceramic composite. The metallic properties of Ag are used to increase the superconductivity properties of HTS. The addition of Ag has been extensively studied and reported to have an impact on the electrical, structural and mechanical properties of $YBa_2Cu_3O_7$ bulk materials. Based on the crystal structure of $YBa_2Cu_3O_7$, the lattice parameter of the orthorhombic unit cell, *a*-axis and *c*-axis will increase with increasing Ag concentration. Meanwhile, the lattice parameter for *b*-axis remains the same for all the sample with different Ag contents (Zhang *et al.,* 1995). The significant of higher *c*-axis will contribute to the improvement of pinning centre without decreasing the critical temperature (T_C).

These changes were linked to the Ag substitution for Cu in $YBa_2Cu_3O_7$ ceramics. Cu and Ag are from the same group of the periodic table of elements that enable Ag atoms to substitute Cu(1) in the Y-123 grains and affect various physical properties. The excellent in chemical compatibility enable the Ag ion to be encountered into the Y-123 (Azambuja *et al*., 2008). The excess metallic Ag will fill the pores of the bulks and encouraged the formation of larger stacks of flat rectangular platelets, resulting in a *c*-axis preferred orientation (Salamati *et al*., 2001). Furthermore, the addition of Ag enhances the critical current density, besides improving the grain growth and helps to obtain a better grain orientation, lowering the electrical resistance in the normal state. In addition, silver addition to Y-123 enhances the process dominated by the weak links. The possible reasons for the

formation of these weak links are composition variations at the grain boundaries and misorientation of grain boundaries (Benzia *et al.,* 2004).

Next, the small value of the grain boundary critical current density in polycrystalline samples is known as a problem for large-current applications. It can be solved by grain alignment and optimization of the microstructure to minimize the effective grain-boundary area. The effective ways to minimize the grain boundary area is to increase the size of superconducting grains (Rani *et al.,* 2013). Ag in bulk YBCO superconductors significantly improves the grains coupling, and as a result, it will optimize the superconductivity performance. It has been found that Ag reduces the normal-state-resistivity, enhances magnetic-flux trapping, decrease the contact resistance, improve electrical stability, and resistance to water as well. Besides, Ag addition also affects the mechanical properties in term of its ductility, flexural, strength, and toughness of the YBCO (Zhang *et al*., 1995).

CHAPTER 3

MATERIALS AND METHODS

3.1 Materials

The raw materials used in the research consist of Yttrium oxide (Y_2O_3), Barium Carbonate ($BaCO_3$), Copper Oxide **(**CuO) which uses to synthesize pure $YBa_2Cu_3O_7$. Besides, the use of Al_2O_3 addition towards the $YBa_2Cu_3O_7$ with different weight percentages (x : Al_2O_3 : 0.00, 0.10, 0.20, 0.50, 1.5, 3.5 wt%) in chemical powder form. The list for raw materials that will be used in the preparation of $YBa_2Cu_3O_7$ with Al_2O_3 nanoparticles was shown in table 3.1 as below.

Table 3.1: The raw materials used in the preparation of YBCO with Al_2O_3 nanoparticles addition (x : 0.00, 0.10, 0.20, 0.50, 1.50, 3.50 wt%).

No.	Materials (chemical powder)
1	Y_2O_3
2	$BaCO_3$
3	CuO
4	Al_2O_3

3.2 Methods

3.2.1 Synthesis of Pure $YBa_2Cu_3O_7$

High-temperature superconductors was prepared by solid state reaction method. It is a conventional solid state reaction conducted by a chemical route which involves a series and step of the method which consists of chemical mixing, calcination, the intermediate firing, and oxygen annealing. This process takes place at a high temperature, where the chemical powder was mixed into a powder form and pressed into pellets. YBCO was prepared by mixing the chemicals as per balanced chemical equation shows in 3.1 as below.

$$\frac{1}{2}\,Y_2O_3 + 2BaCO_3 + 3CuO \rightarrow YBa_2Cu_3O_7 + 2CO_2 \qquad (3.1)$$

Yttrium oxide, Barium Carbonate, Copper Oxide is taken in a stoichiometric ratio (1:2:3) to prepare YBCO. The raw material was measured using the high precision balance correct up to 4 decimal places. The mixed sample was grounded by using ball milling for nearly 2 hours so as to obtain a homogenous mixed powder of the raw materials. The mixture was removed after the temperature reach room temperature.

3.2.2 Calculation for $YBa_2Cu_3O_7$ Preparation

The Atomic Mass Unit (AMU) for each component was used to calculate the mixture ratios in producing precise weight for mixture of sample. The AMU for each of the component is shows the table 3.2 as below.

Table 3.2 : The Atomic Mass Unit (AMU) for each component.

Component	The Atomic Mass Unit (AMU)
Yttrium	88.906 g/mol
Barium	137.327g/mol
Copper	63.546 g/mol
Carbon	12.001 g/mol
Oxygen	15.999 g/mol
Calcium	40.078 g/mol

3.2.3 Preparation of $YBa_2Cu_3O_7$ with Al_2O_3 Nanoparticles Addition

The pure YBCO powder will be added with Al_2O_3 nanoparticle in a fixed ratio $YBa_2Cu_3O_7$ + Al_2O_3 (x : 0.00, 0.10, 0.20, 0.50, 1.50, 3.50 wt%). They were grounded individually for one hour each and press in the form of pellets by using pelletizer for powder compaction in 1 g for each sample at 0.6 GPa.

3.2.4 Calcination

Calcination is the heating of a solid to a high elevated temperature, below its melting point in order to create a condition of thermal decomposition or phase transition other than melting or fusing (Schubert & Husing, 2005). It is an endothermic process where a substance is subjected to an elevated temperature (Sadhana *et al.,* 1988). This process helps in removing moisture or unknown composition nor impurities. Besides, it also helps to homogenizing the material as well.

After mixed the materials, the powdered sample was calcined in a furnace for 12 hours at 900°C temperatures. Then the furnace was cooled and the sample was thoroughly grounded to ensure proper mixing which prevent the agglomerates happened in the sample. The heating rate is 5^{o}C/min same as the cooling rate. The heating profile for the calcination process is plotted in figure 3.1. The calcination temperatures are affected by the electrical and mechanical properties of the ceramics to a large extent. Calcination leads to the formation of the desired phase of the superconducting YBCO. This calcination decomposes the carbonates, nitrates or other impurity phases.

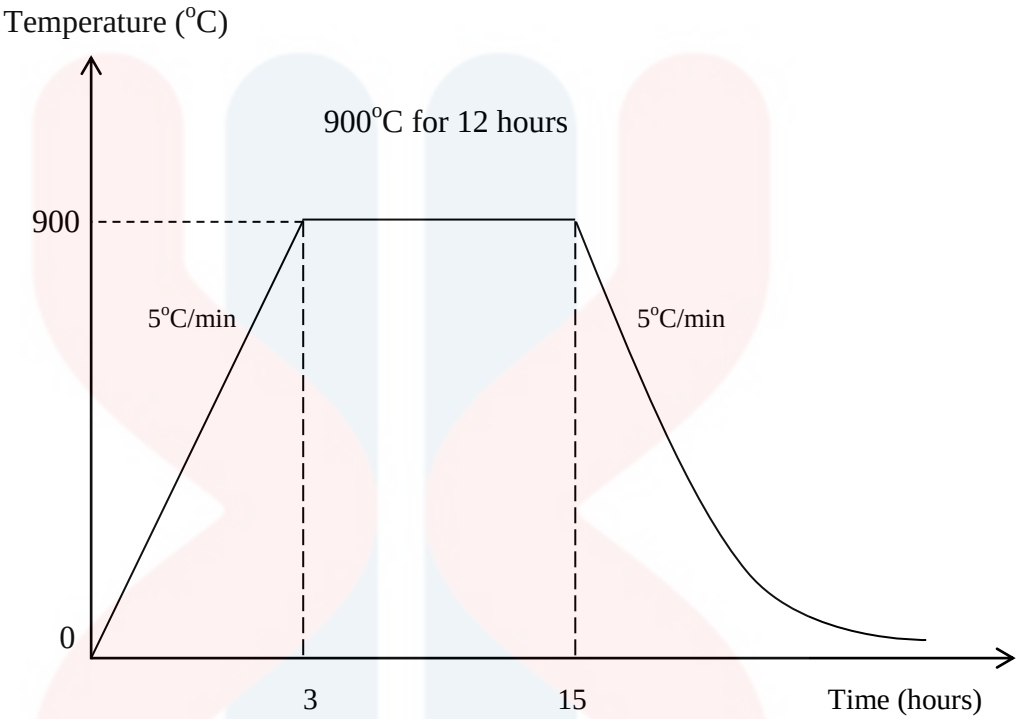

Figure 3.1 : The heating profile for calcination

3.2.5 Sintering

Sintering is a thermal treatment of grain material at a temperature below the melting point in order to increase the grain size and strengthen the bond of the particles together (Menad, 2011). Besides, the thermally activated transition of a powder will decrease the free surface energy (Olevsky, 2011). Sintering may be also refers to the changes in pore shape, pore shrinkage and the increase in grain size that CaO particles undergo during heating. The rate of CaO sintering increases at higher temperatures. The presence of impurities also increases the sintering rate. In general, higher temperatures are required to increase reaction rates, but because of the

sintering process, the structure of the calcination is more likely to change (Liu & Yang, 2015)

For this research, the powder sample was pressed in the form of cylinder-shape pellets of 1 gram each. The pellets were sintered in a conventional furnace at 950^{o}C for 12 hours and annealed in the presence of oxygen. Next, the heating rate is 5^{o}C/min same as the cooling rate. The heating rate for the sintering process was shown in figure 3.2. In the sintering stage the pellet shaped sample was heated to produce the desired microstructure by the reduction in grain boundary volume and increase in particle contact region.

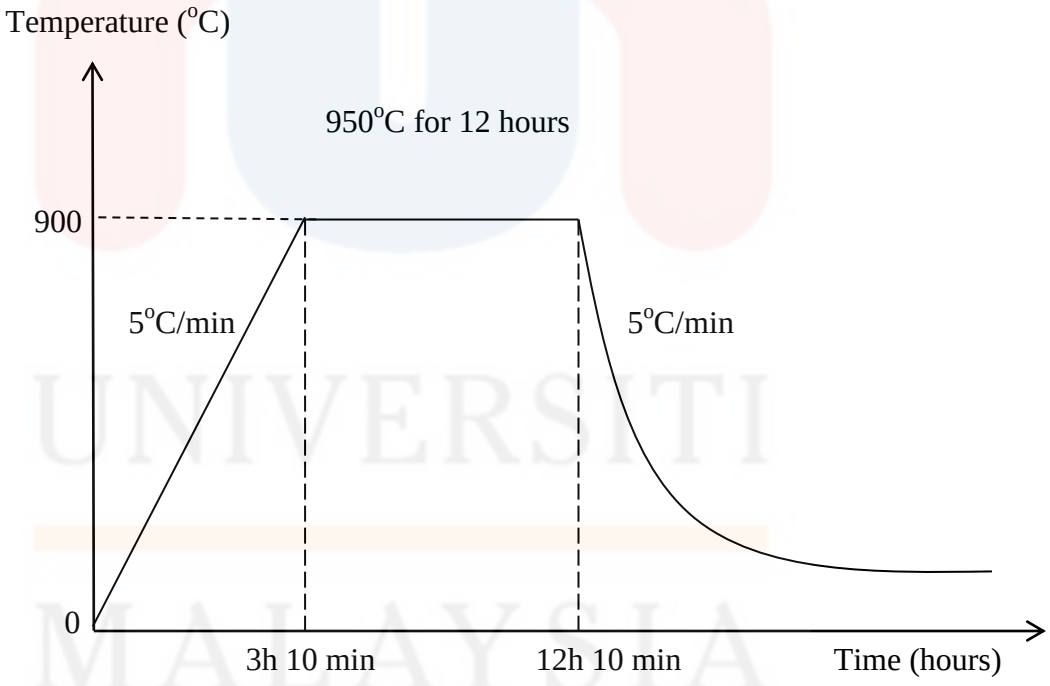

Figure 3.2 : The heating profile for sintering

3.2.6 Annealing

Annealing is a simple process that involve a disclosement of material to a temperature for an extended time, followed by a slow rate of heat treatment to be cooled (Rajan *et al.,* 2011). However, this process may also alter the chemical and physical properties of sample for specific performance. This process enhances the toughness and ductility of a material. Besides, the internal stresses during the process of solidification can be relieves by annealing process. The grain size can be refines and the reduction content of gaseous. Bases on the research, annealing process was be done by slow cool rate to room temperature at 5^{o}C/min.

3.3 Schematic Diagram

The schematic diagram shown the whole significant process and steps which werw involves in preparing the high-temperature ceramic superconductors of $YBa_2Cu_3O_7$ by solid state reaction method. For figure 3.3, the schematic diagram shows from mixing to the calcination process in synthesizing pure YBCO powder. Besides, the process from Al_2O_3 nanoparticles addition, powder compaction and sintering process was being detailed in the schematic diagram for figure 3.4.

For the flowchart diagram, the chemical powder of Y_2O_3, $BaCO_3$, CuO in the ratio of (1:2:3) was mixed and calcined at elevated temperature. Then, the pure YBCO powder was involved in the second mixing with the addition of Al_2O_3 nanoparticles (x : 0.00, 0.10, 0.20, 0.50, 1.50, 3.50 wt%). Next, the chemical powder was compacted in a cylindrical pallet of samples and sintered. The flowchart diagram for the research is shows in figure 3.5.

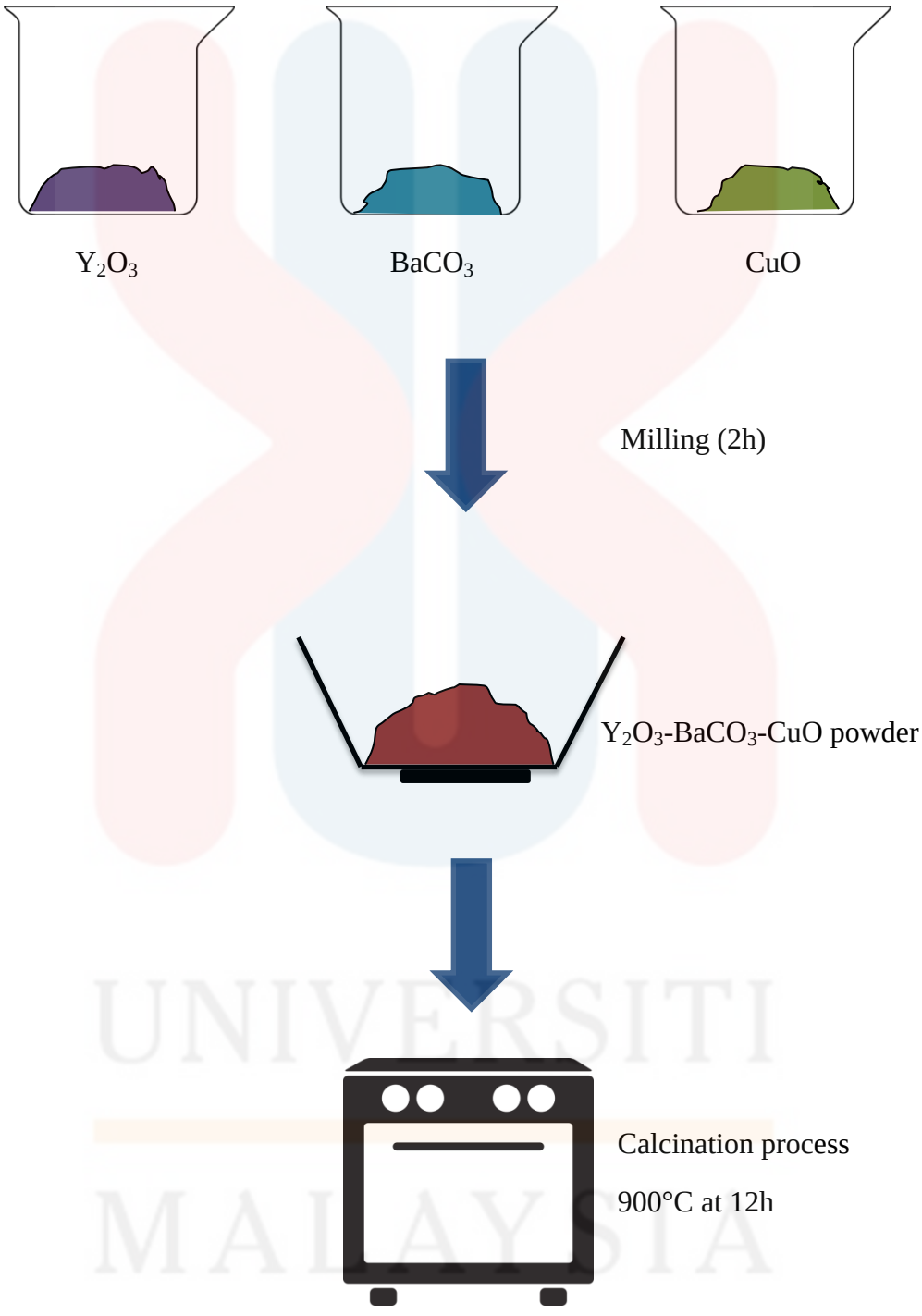

Figure 3.3 : The schematic diagram from mixing to calcination process.

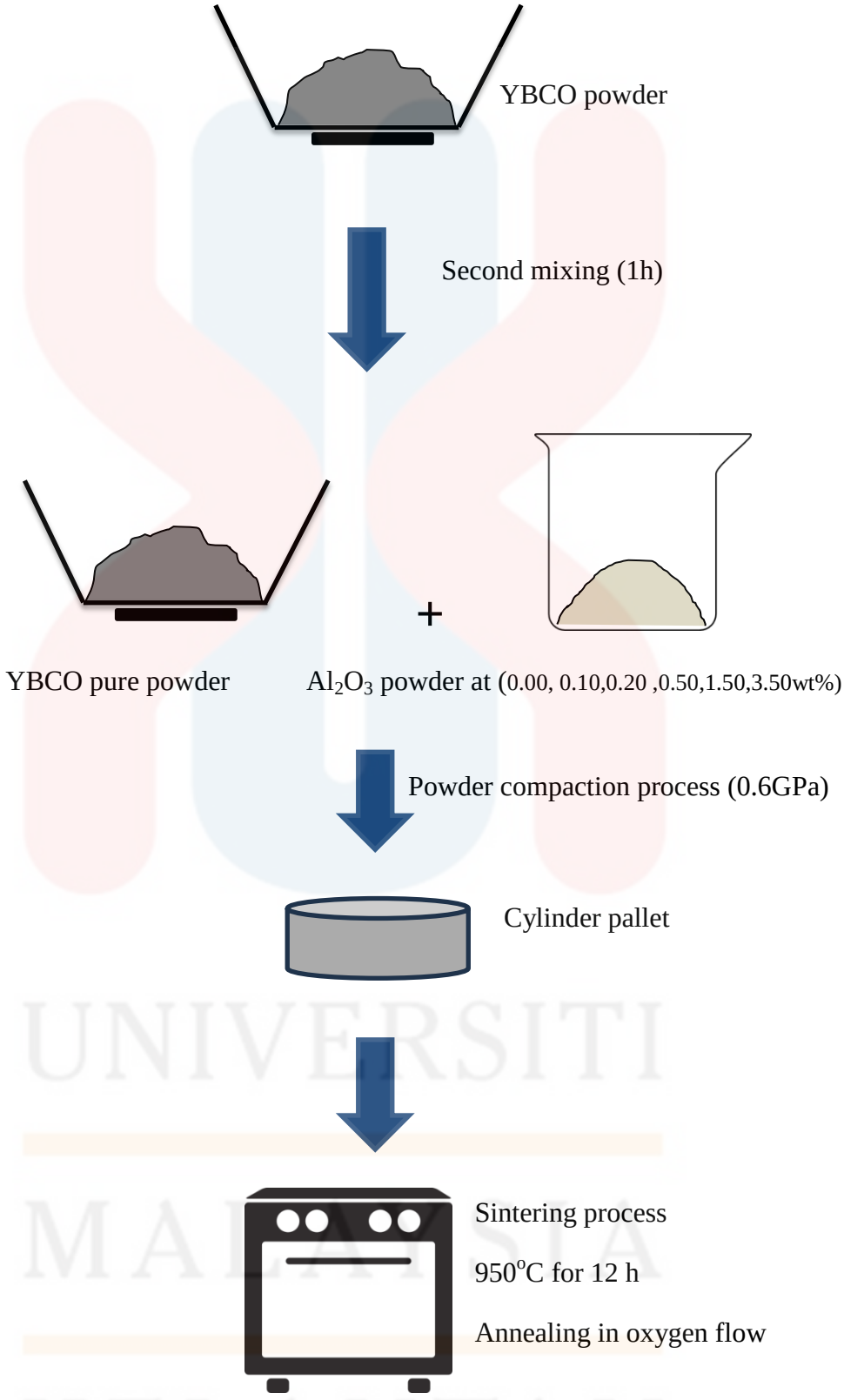

Figure 3.4 : The schematic diagram from addition of Al_2O_3 to sintering process.

3.4 Research Flow Chart

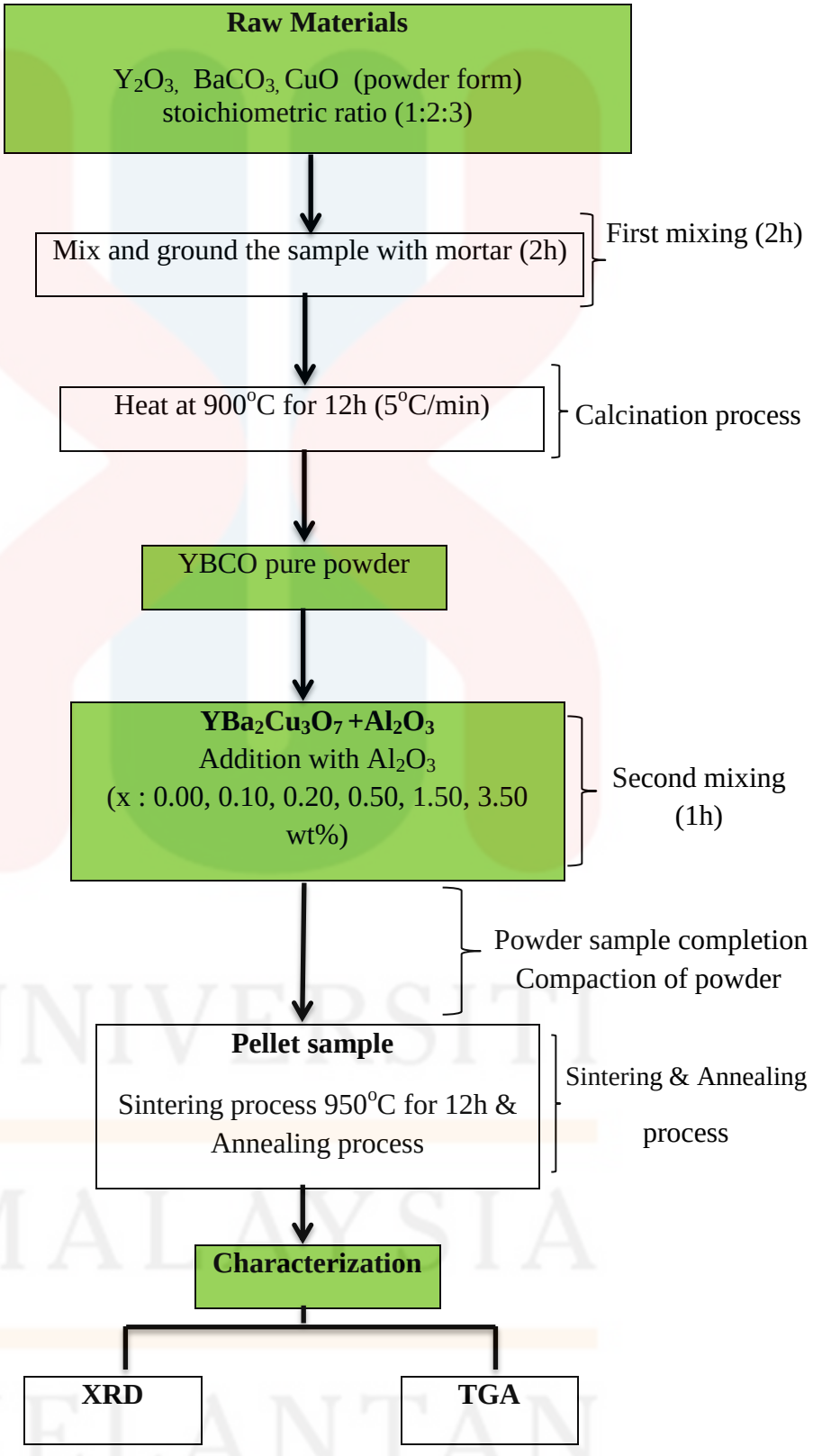

Figure 3.5 : The flowchart diagram for the research.

3.5.0 Characterization Method

3.5.1 Crystal Structure Analysis by XRD

The structural development of the produced samples was investigated using X-ray diffraction patterns, recorded using the Cu Kα irradiation (wavelength, = 1.54184 Å) and the scanning range was between 10° and 90°. This technique was used to determine the phase for crystalline materials in providing vital information on the unit cell. Besides, the data was used to examine the changes in the parameters of the crystal structure. The intensity peaks of Al_2O_3 will be observed in YBCO samples, in particular for higher Al_2O_3 content samples.

Diffraction patterns are observed when X-Ray of wavelength (λ) interacts with the atomic arrangement of atoms comparable with the interplanar spacing (d) of crystals, satisfying the Bragg condition by using the equation 3.2. The scattered X-rays from the planes interfere constructively only when the path difference is an integral multiple of the X-ray wavelength. Here 'n' is the order of diffraction, 'd' is the interplanar distance for the set of parallel planes with Miller index (hkl) that gives a diffraction peak at a particular Bragg angle for orthorhombic system.

$$2dsin\theta = n\theta \qquad (3.2)$$

X-ray powder diffraction pattern yields the following information:

(i) Phase confirmation and quality of the synthesized samples

(ii) The interplanar spacing ‘d’ of the system under investigation.

(iii) The intensities of the reflections.

(iv) The lattice type and unit cell dimensions.

3.5.2 Particle Size Measurements

The XRD profile was used to measure the average crystal size in the sample. The particle size for YBCO with Al_2O_3 addition will be calculated from X-ray diffraction profiles with intensity% by measuring the Full Width at Half Maximum (FWHM) from the data given. The Debye Scherrer equation was used in calculating the particle size shows in equation 3.2 (West, 1974).

$$D = \frac{K\lambda}{\beta \cos\theta} \tag{3.3}$$

K is the Scherrer constant, λ is the wavelength of light used for the diffraction, β is the “full width at half maximum” of the sharp peaks, and θ is the angle measured.

3.5.3 Instrumental Broadening

The broadening in X-ray diffraction lines was occurred when the particle size is less than 100 nm. The particle size and strain was the factor for having a diffraction pattern and broadening. Besides, the broadening of peak may also occur due to micro strains of the crystal structure which originally due to defect, such as dislocation and twinning (Ghosh *et al.*, 2014). Furthermore, the total broadening of the diffraction peak was due to sample and the instruments. The line broadening will was used to estimate the average size of the particles.

3.5.4 Thermal Analysis

In Differential thermal analysis (DTA/TGA), the material and an inert reference are made to undergo identical thermal cycles. The thermal analysis will record any temperature difference between sample and reference. The result for the differential temperature will be plotted against temperature, or against time. Any changes for exothermic or endothermic reaction will be detected within the sample relative to the inert reference. Thus, the transformations such as glass transitions, crystallization, melting and sublimation occurred will be provided as DTA curve data (Bhadeshia, 2002).

CHAPTER 4

RESULT AND DISCUSSION

4.1 Introduction

In this chapter, section is focussed on the on the discussion of the synthesized of $YBa_2Cu_3O_7$ with the reaction of Al_2O_3 nanoparticles addition. Thus, the samples was divided to six different weight percentages of addition Al_2O_3 (x : 0.00, 0.10, 0.20, 0.50, 1.50, 3.50 wt%) which have six sample for all. The effect of Al_2O_3 nanoparticles addition with respect to Cu atoms that will produce a compound of orthorhombic structure is studied. The lattice parameter, orthorhombicity, lattice strain and crystallite size were included as the outcomes for the X-Ray powder diffraction (XRD) testing.

4.2 X-Ray Diffraction Characterization for Before and After Calcination Process in $YBa_2Cu_3O_7$ Synthesis.

4.2.1 X-Ray Diffraction Before Calcination Process.

The X-ray diffraction analysis was performed for sample including before and after calcination process. The phase identification was carried out using X-ray diffraction with Cu Kα radiation. The XRD pattern of sample $YBa_2Cu_3O_7$ before calcination process was shown in figure 4.1. Those data was compared in order to determine the stuctural parameter. The dominant elements pattern that were studied in this section are the Yttrium oxide (Y_2O_3), Barium carbonate ($BaCO_3$) and Copper oxide (CuO) powder. The intensity and the peak position of reflection for the result

are in good agreement with the values reported. It is clear that the relative intensity and peak position is different between the before and after calcination process.

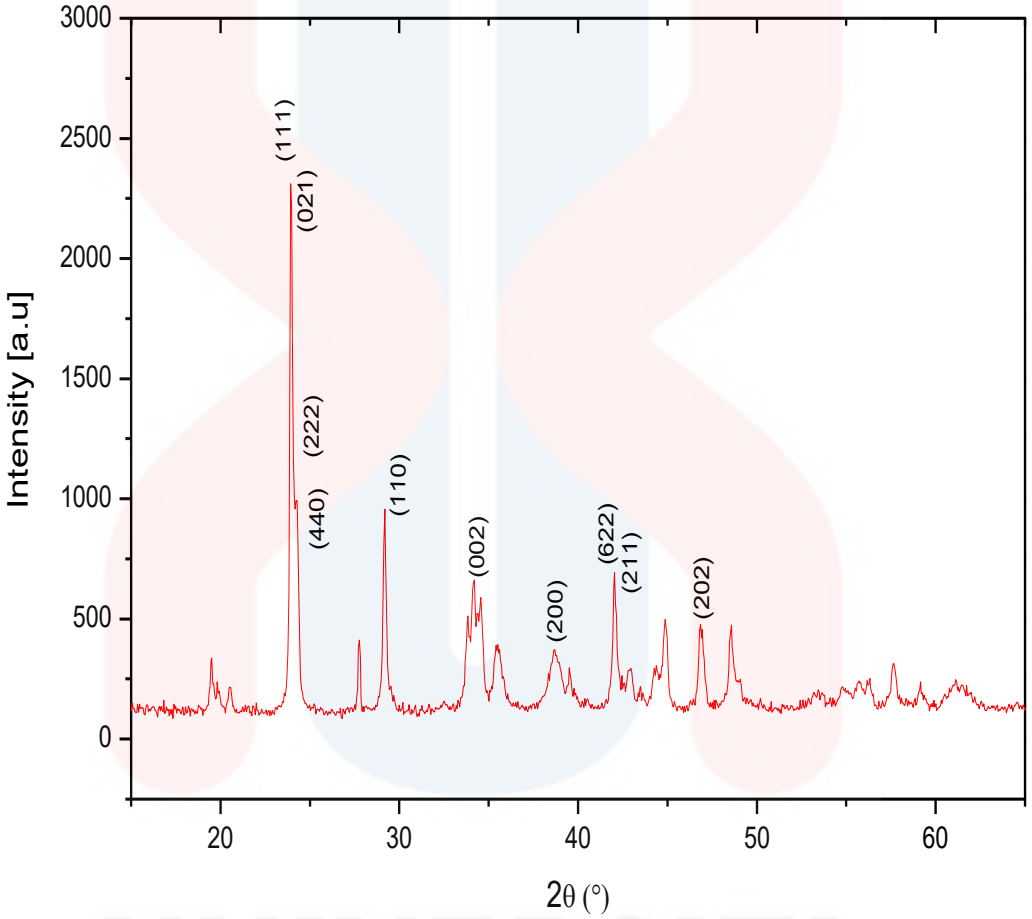

Figure 4.1 : The XRD pattern of sample $YBa_2Cu_3O_7$ before calcination process.

The Bragg's peaks of the crystallized powders correspond to each sample agree well with the reflections of pure orthorhombic $BaCO_3$ single phase with a = 5.314 Å, b = 8.904 Å and c = 6.4284 Å. The XRD patterns show that the intensities of three basic peaks of the (111), (021) and (211) planes for Barium carbonate is formed (Bagheri *et. al.*, 2008).

Table 4.1 show the XRD patterns for $BaCO_3$ crystallography orientations before calcination process.

Table 4.1 : The XRD patterns for $BaCO_3$ crystallography orientations before calcination process.

hkl	2θ	Intensity	d (Å)
111	24.20	2020	3.70
021	24.95	1072	3.64
211	42.50	627	2.14

The XRD pattern in CuO as diffraction peaks for the monoclinic phase was exist. The characteristic peaks located at 2θ = 32.58°, 35.47°, 38.97° and 48. 74° are assigned to (110), (002), (200) and (202) plane orientation of CuO. The lattice parameters prove that a = 4.6837 Å, b = 3.4226 Å and c = 5.1288 Å. Table 4.2 show the XRD patterns for CuO crystallography orientations before calcination process.

Table 4.2 : The XRD patterns for CuO crystallography orientations before calcination process.

hkl	2θ	Intensity	d (Å)
110	32.57	143	2.75
002	35.47	239	2.53
200	38.97	219	2.31
202	48.74	233	1.87

As for Y_2O_3, the characteristic peaks located at 2θ = 24.20, 24.95, and 42.50. The XRD patterns show that the intensities of three basic peaks of the (2 2 2), (4 4 0) and (6 2 2) planes are more than of others peaks. Thus, the table 4.2 below show the XRD patterns for Y_2O_3 crystallography orientations before calcination process.

Table 4.3 : The XRD patterns for Y_2O_3 crystallography orientations before calcination process.

hkl	2θ	Intensity	d (Å)
222	24.20	944	3.06
440	24.95	479	1.87
622	42.50	367	1.60

4.2.2 X-Ray Diffraction After Calcination Process.

The XRD pattern of $YBa_2Cu_3O_7$ after the calcination process shows different intensity between the raw material and additional phase which was created after the calcination process. Thus, the additional phase exist was Y-211 at 2θ = 29.82^o and 30.50^o. The additional phase may due to the heating reaction, grinding cycle and results in poor homogenity plus with large particle size (Kumar et al., 1993). CuO was indistinctly appeared but the presence of CuO peaks was stronger occurred after calcinations process. Besides, $BaCO_3$ peaks also getting stronger after the calcination process. The width of the strongest peak decreases with increasing of the calcination temperature, which refers to the growth of crystal size and also the intensity of the peaks increase which leads to the more crystalline structure (Bagheri *et. al.*, 2008). Furthermore, the XRD peaks sharpened after calcination temperature, indicating crystallite growth (Larimi *et al*., 2011). Besides, peak broadening is due to micro

strain with different types of micro strain. Moreover, peak broadening is may causes by solid inhomogeneity, temperature factors and crystallite size. Next, the broadening of peak may also occur due to micro strains of the crystal structure which originally due to defect, such as twinning and dislocation (Ghosh *et al.*, 2014). The figure 4.2 below shows the XRD pattern of sample $YBa_2Cu_3O_7$ before and after calcination process.

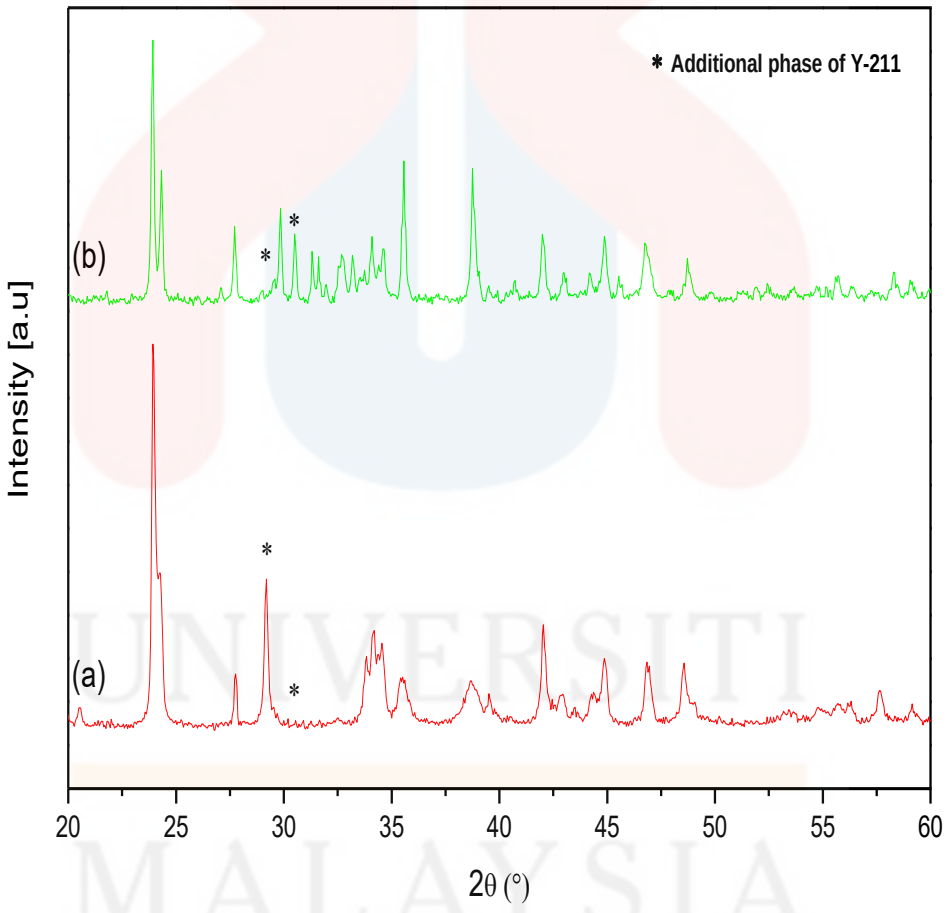

Figure 4.2 : The XRD pattern of sample $YBa_2Cu_3O_7$ (a) before (b) after calcination process.

4.2.3 X-Ray Diffraction Characterization for $YBa_2Cu_3O_7$ After Sintering Process.

Details of the structural changes associated with the addition of nanoparticles Al_2O_3 and the related a lot of properties that have already been reported elsewhere such electrical resistivity and critical transition temperature (Schilling *et al.*, 1993). For all $YBa_2Cu_3O_7$ that was added with Al_2O_3 nanoparticles, the X-ray diffraction patterns show the usual orthorhombic structure with Pmmm symmetry and an insignificant quantity of additional phases in sample. Thus, all the samples can be indexted to Y-123 with the highest dominant peaks of (103) and (013). Besides, the presence of other phase is not affected by the Al_2O_3 nanoparticles addition. The XRD patterns of pure Y-123 along with Al_2O_3 nanoparticles addition have been shown in figure 4.3. It is clear to see that the intensity for YBCO increases at elevated addition of Al_2O_3 nanoparticles. There was some additional phase which may occurred due to the twining defect of tetragonal to orthorhombic phase transformation. Below 750^0C, the sample undergoes a tetragonal to orthorhombic structural phase transition, resulting in twinning on the (110) or the perpendicular planes. Twins are formed to reduce strain energy due to the change in shape and volume of the unit cell resulting from the phase transformation (Khoshnevisan, 2002).

The Al_2O_3 characteristic peaks, however, were unable to be distinguished from the background noise peaks because of relatively low Al_2O_3 nanoparticles content and highly dominant of $YBa_2Cu_3O_7$ peaks (Suan & Johan, 2014). These values are comparable with the literature of the pure $YBa_2Cu_3O_{7.}$ At these compositions, the $YBa_2Cu_3O_7$ lattice structure remained unchanged because the

Al_2O_3 nanoparticles were yielded as the distinct phases and well distributed in the samples. The same additional phase that exist in the sample after calcination does not shows any changes in term of intensity with increases addition of Al_2O_3 nanoparticles (Widad & Salwan, 2012). The lattice constant parameters for prepared specimens are nearly same with average values of a = 3.821 Å, b = 3.880 Å and c =11.663 Å which are comparable with the literature for Y-123 (Benzia *et al*, 2004). The addition samples did not show any changes in terms of structural properties and is quite similar as observed in the XRD patterns of pure YBCO. This is attributed to the fact that in these compositions Al_2O_3 nanoparticles were existed as another phase and uniformly distributed in YBCO matrix (Suan & Johan, 2013). Thus, the table 4.4 shows the unit cell parameter and the unit cell volume for $YBa_2Cu_3O_7$ with Al_2O_3 nanoparticles addition. There are no orthorhombic to tetragonal phase transformation occurred with the presence of higher Al_2O_3 nanoparticles addition in Y-123.

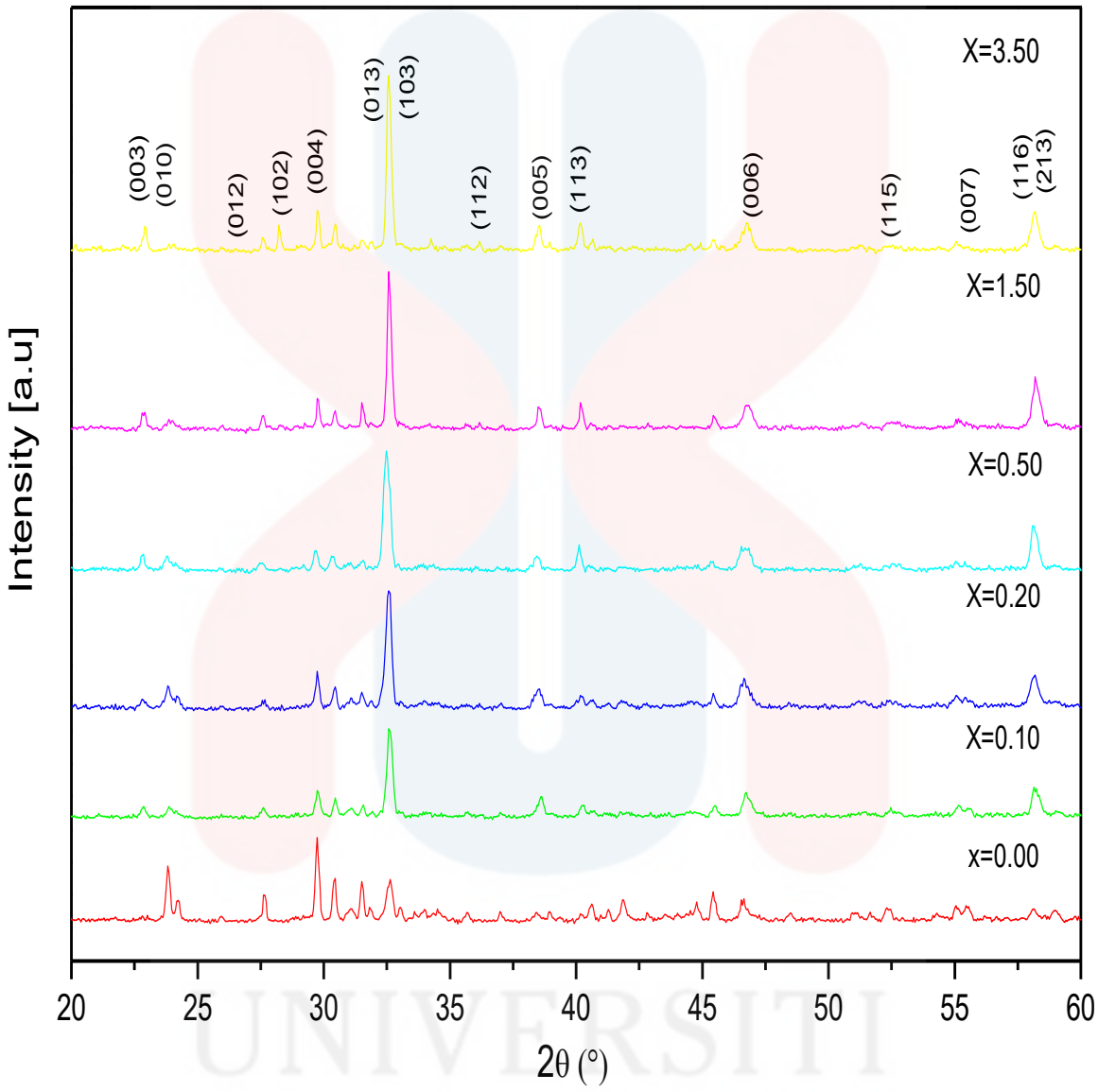

Figure 4.3 : X-ray diffraction of $YBa_2Cu_3O_7$ with Al_2O_3 nanoparticles addition

(X= 0.00, 0.10, 0.20, 0.50, 1.50, 3.50 wt%)

It is expected that the *a* and *c* parameter increase slightly in higher amounts of Al_2O_3 addition whereas *b* parameter almost remains constant. The *a* and *c* lattice parameters are noticed to increase as the Al_2O_3 nanoparticles content was increased in samples. The increments are believed because O^{2-} ions try to fill in its deficiencies site and incorporation of Al^{3+} ions at the Y site (Suan & Johan, 2014). These alterations illustrate that the Al^{3+} ions occupy in both Y and Cu sites. The addition of nanoparticles Al_2O_3 slightly decreases the difference between *a* and *b* parameters and thus reduces the orthorhombicity. According to the reflections related to the XRD patterns (hkl), it can be deduce that (013) and (103) peaks merged together and with increment of Al_2O_3 nanoparticles addition. The (103) reflection tends to be lowered in angle that lead to the decreases of orthorhombicity in the system (Mellekh *et al*., 2006). It can be noticed that the volume of unit cell increases with the elevated addition of Al_2O_3 nanoparticles and that is attributed to the effect of Al-substitution on the variation of the lattice parameters.

Table 4.4 : The unit cell parameter and the unit cell volume for $YBa_2Cu_3O_7$ with Al_2O_3 addition.

Al_2O_3 addition (wt%)	Cell Parameters			V(Å^3)
	a (Å)	*b* (Å)	*c* (Å)	
0.00	3.8410	3.8830	11.6710	174.0683
0.10	3.8424	3.8810	11.6821	174.2076
0.20	3.8177	3.8836	11.6827	173.2126
0.50	3.8360	3.8830	11.6860	174.0652
1.50	3.8250	3.8864	11.6945	173.8443
3.50	3.8184	3.8857	11.7010	173.6096

Figure 4.4 represent the evolution of lattice parameters versus Al_2O_3 nanoparticles addition, where the *a* and *c* shows the increment in their lattice parameter. Meanwhile, for *b* parameter in all addition of Al_2O_3 nanoparticles remain stable and almost constant.

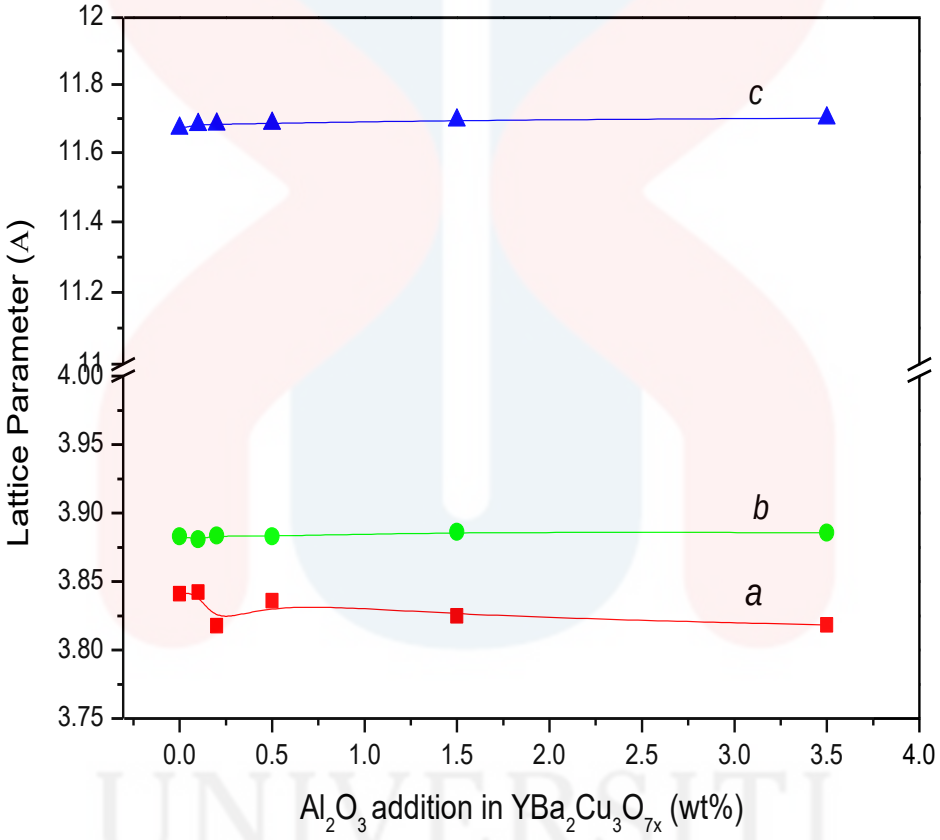

Figure 4.4 : Evolution of lattice parameters(Å) versus Al_2O_3 nanoparticles addition (wt%)

Thus, the orthorhombicity with different Al_2O_3 nanoparticles addition in $YBa_2Cu_3O_7$ was caclculated by using the formula from equation 4.1 (Giri *et al.*,2005). The *a* and *b* in the formula indicating the lattice parameters.

$$\frac{(b-a)}{(b+a)} \tag{4.1}$$

The increasing weight percentage of Al_2O_3 addition, the orthorhombicity is decreased from x = 0.00 to 0.10 and x = 0.20 to 0.50 due to the weakend binding in CuO chain as reflected in the oxygen vacancies disorder (Bandyopadyey *et al.,* 1997). There is a sudden increase at x = 0.10 to 0.20 and x = 1.50 to 3.50 which indicate the overdoped region in the system. The addition of Al_2O_3 nanoparticles slightly decreases the difference between *a* and *b* parameters and thus reduces the orthorhombicity. On top of that, with the increasing of Al_2O_3 nanoparticles addition indicates that the orthorhombicity of the system decreases. The slow variation in the *a* parameter and the changes in the unit cell volume with increasing Al_2O_3 nanoparticles addition level most probably indicate that Al is incorporated into the crystal structure (Sahoo & Behera, 2012). The figure 4.5 below represent the orthorhombicity caclculation with different Al_2O_3 content addition in $YBa_2Cu_3O_7$.

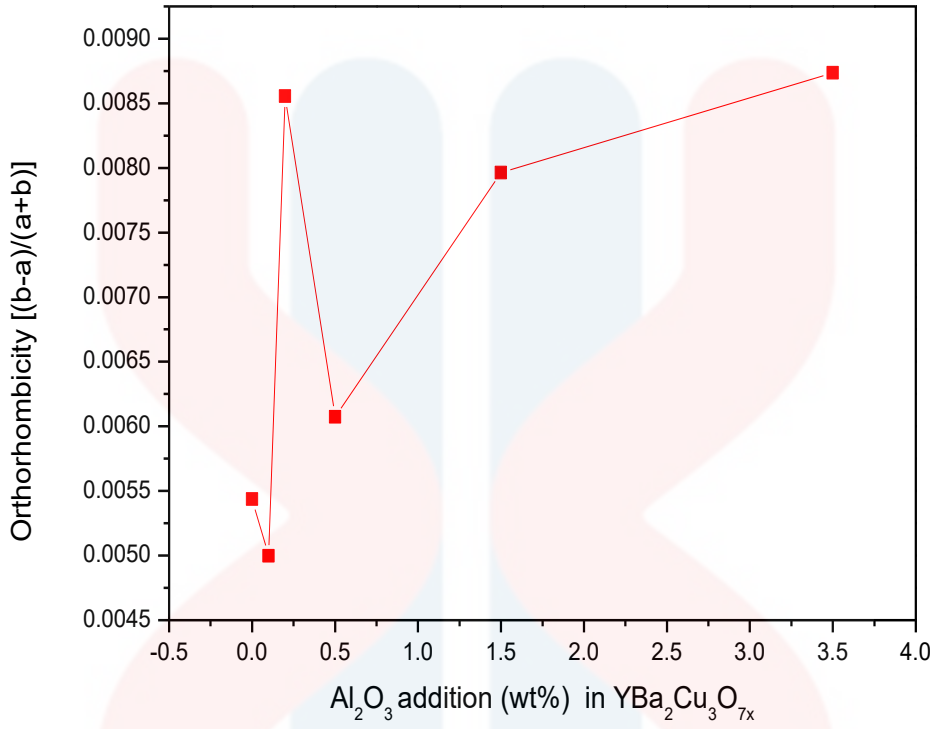

Figure 4.5 : The orthorhombicity caclculation with different Al_2O_3 content addition in $YBa_2Cu_3O_{7.}$

Moreover, there was an effect of lattice strain in the sample. The volumetric strain can be divided into two parts which are strain due to bond distance change and strain due to vacancy sources and sinks. It causes the broadening with due to lattice strain in the material (Li *et al*., 2016). Besides, the lattice strain may due to the formation of misfit dislocation in the sample. The lattice strain was causes by the decreasing of weak-link at the grain boundaries. It is causes by the improved grain alignment with the addition of Al_2O_3 nanoparticles (Sukirman *et al.*, 2007).

4.3 The Crystallite Size of $YBa_2Cu_3O_7$ with Al_2O_3 Nanoparticles Addition

The crystallite sizes of the samples after sintering process was calculated from the width of the selected peak and half-maximum as listed in table below. The crystallite size of YBCO powder yielded from the solid state reaction was about 31.59 nm. The crystallite size was increased to 34.72 nm and 34.47 nm with the addition of 0.10 and 0.20 wt% of Al_2O_3 nanoparticles in sample. At 0.50 wt%, the crystallite size shows nanoparticles addition was 1.50 wt%. The graph of figure 4.6 below shows Al_2O_3 nanoparticles addition (wt%) versus the crystallite size (nm). These changes were possibly due to the existence of thermally stable Al_2O_3 nanoparticles that impeded the grain growth of YBCO powder during sintering process. Thus, the Al_2O_3 nanoparticles were believed to be agglomerated at the grain boundaries and provide a pack of Al^{3+} ions which easily diffused into the YBCO structure (Suan & Johan, 2013). However, the addition of Al_2O_3 nanoparticles at 0.50wt% produced the lowest crystalline size, 28.14 nm. Thus, the decrease of crystallite size will generate a change in physical properties dramatically (Sukirman *et al*., 2009). The table 4.5 shows the crystallite size with Al_2O_{3x} addition (wt%).

Table 4.5 : The crystallite size of sample with Al_2O_3 addition (wt%)

Al_2O_3 addition (wt%)	Crystallite size, D (nm)
0.00	31.59
0.10	34.72
0.20	34.47
0.50	28.14
1.50	44.82
3.50	41.66

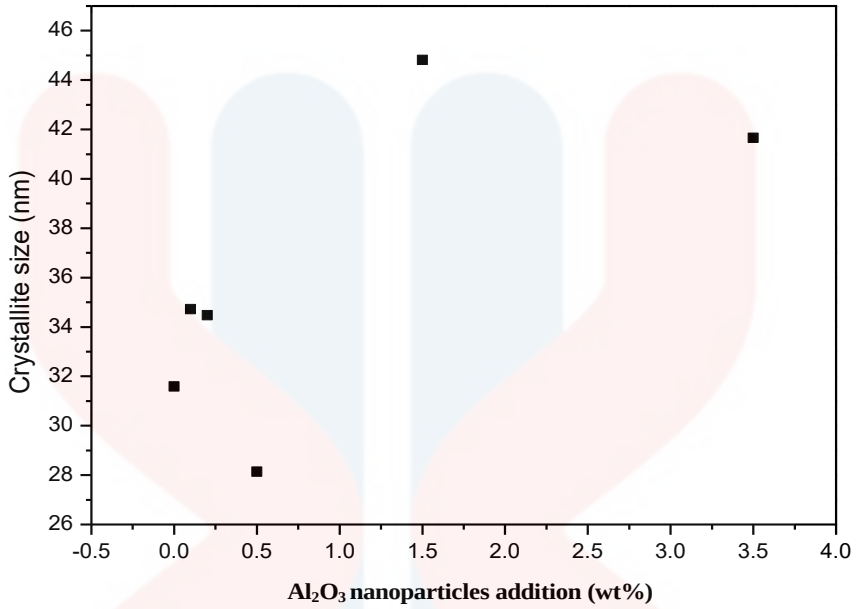

Figure 4.6 : The Al_2O_3 nanoparticles addition (wt%) versus the crystallite size (nm)

4.4 Thermal Analysis by Thermogravimetric Analyzer (TGA)

Thermogravimetric Analyzer (TGA) can detect the weight change of a material as a function of temperature. This method can therefore measure the shifts in weight associated with the oxidation and reduction of Yttrium- Barium-Copper-Oxide. Thermogravimetric Analyzer was used to condition the HTSC material to different oxygen levels. It has been applied to the study of oxygen diffusion in YBCO powder and polycrystalline samples of varying density. The use of single crystals with this method has not been reported, perhaps due to the difficulty in producing the large amount of crystals needed so that the data from the weight measurements is outside the experimental error region inherent to the system used.

4.4.2 Thermal Analysis for YBCO Before Calcination Process.

Thermogravimetric analyzer (TGA) show the TGA curve at temperatures up to 1000 ºC although TGA analysis indicated weight loss was complete by 920 ºC. The phase purity of YBCO powders observed by XRD shows at temperatures 900 ºC to 920 ºC, suggesting a stable end product of YBCO with high purity was achieved via solid-state reaction. The result shows the decomposition for bulk powders specimens by forming TGA analysis. Figure 4.7 below shows the TGA curve of YBCO sample before calcination process. In this technique for the study of YBCO, the synthesis of the sample was determined by following the weight of the sample as a function of temperature from 200 to 1000 ^{0}C with heating gradient of 5 ^{0}C/min in a an open air. Base on the research by Khoshnevisan; 2002, there was a no any weight change until 400 ^{0}C and after that different reaction carried out. However, from 196.45 to 346.73 ^{0}C, there was a weight change of 0.32% for 0.247mg from the sample powder which indicating some impurities exist in the sample. Meanwhile, from 346.81 to 995.62 ^{0}C, the weight change was at 13.14% for 10.158 mg. From the temperature of 900 to 920 ^{0}C, the sample show a stabilize end product which is comparable to past research from (Suan & Johan, 2013).

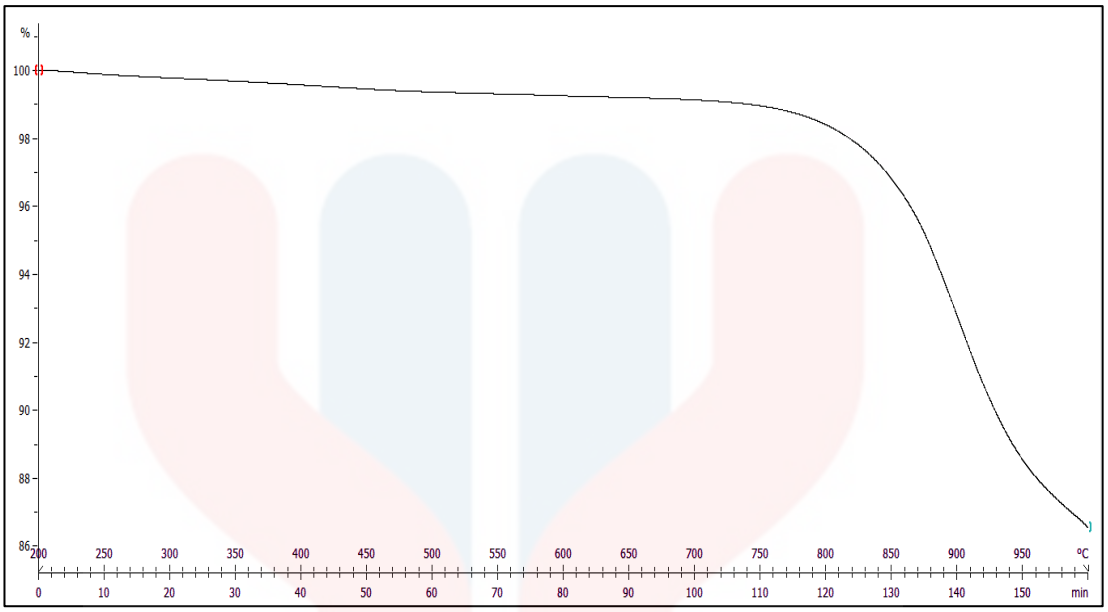

Figure 4.7 : The TGA curve of YBCO sample before calcination process

4.4.3 Thermal Analysis for YBCO with Al_2O_3 Nanoparticles Addition

The sample of YBCO with the addition of Al_2O_3 nanoparticles show in the figure 4.8 below, where the TGA curve shows the formation of YBCO at the range temperature of 900 to 950^{0}C. From 240 to 900^{0}C the intermediate product was stable. The Y_2O_3, $BaCO_3$ and CuO powder after this massive weight loss were stable up to 900^{0}C. Beyond 900^{0}C, the raw materials became non-stable and believed to be reactive in forming YBCO pure powder at 920^{0}C by removing CO_2. On the other hand, the Al_2O_3 nanoparticles stayed as it was and did not involve in any reaction because it is very stable in that temperature range as a ceramic material (Singh *et al*., 2007). The equation 4.2 shows the chemical reaction in producing a stable YBCO powder with the addition of Al_2O_3 nanoparticles. Furthermore, from temperature range of 920 to 950^{0}C, the final product was stabilized and growth of $YBa_2Cu_3O_7$ with Al_2O_3 nanoparticles powder addition. Table 4.6 below shows the

reactions involved in weight loss of YBCO with Al_2O_3 nanoparticles addition at specified temperature.

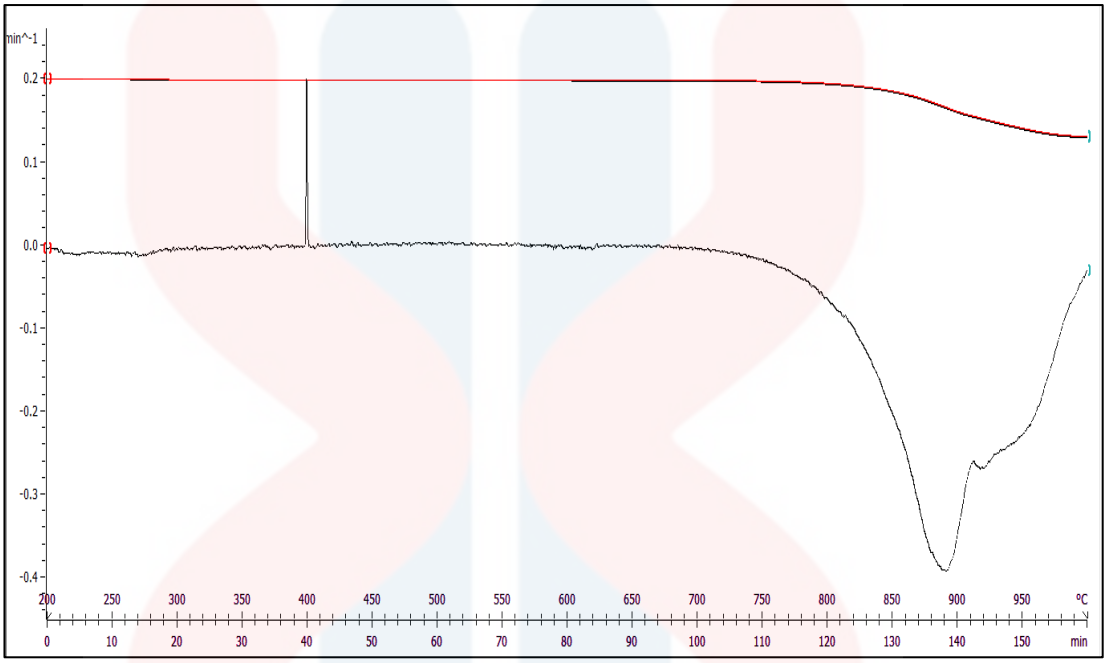

Figure 4.8. : The TGA curve of YBCO with Al_2O_3 nanoparticles addition

Table 4.6 : The reactions involved in weight loss of YBCO with Al_2O_3 nanoparticles addition at specified temperature

Temperature range (^{0}C)	Weight Loss(wt%)	Final Weight(wt%)	Reaction
240-900	–	–	Intermediate product stabilize and growth
900-920	2.0- 4.0	22.0 -26.6	Formation of YBCO + Al_2O_3 with the elimination of CO_2 : $\frac{1}{2}Y_2O_3 + 2BaCO_3 + 3CuO + Al_2O_3 \rightarrow YBa_2Cu_3O_7 + Al_2O_3 + 2CO_2$ (4.2)
920-950	–	22.1- 26.2	Final product stabilize and growth of $YBa_2Cu_3O_7$ with Al_2O_3 nanoparticles powder addition

CHAPTER 5

CONCLUSION AND RECOMMENDATION

In this work, the YBCO pure powder was successfully synthesized and confirmed its phase and quality of the samples. On top of that, Al_2O_3 nanoparticles addition were successfully introduced and well distributed into YBCO superconductor through solid state reaction. In this paper a systematic study on the addition of Al_2O_3 nanoparticles with different weight percentage to $YBa_2Cu_3O_7$ was studied and the orthorhombic structure do not shows any change in the superconducting YBCO compound due to Al addition. There are few additional peaks located at $2\theta = 29.82^o$ and 30.50^o, compare to pure YBCO. Thus, the XRD results can be indexed to Y-123 phase with the highest dominant peaks of (103) and (013) correspond to orthorhombic phase in all samples. Besides, the Y-211 phase appeared slightly in all samples with Al_2O_3 nanoparticles addition with the same intensity trough all sample. The addition of Al_2O_3 nanoparticles lead to the variation of *a* and *c* lattice parameter, whereas b remain constant. The addition in 3.50 wt% shows the highest *c* parameter, 11.7010 Å which is significant in contributing to the improvement of pinning centre without decreasing the critical temperature (T_c). Besides, with the increment of Al_2O_3 nanoparticles also cause the lowering of orthorhombicity of the sample. The increment of Al_2O_3 nanoparticles addition indicates that the orthorhombicity of the system decreases. Furthermore, the addition of 0.50 wt% of Al_2O_3 nanoparticles addition produces smallest the crystallite size of 28.14 nm. From the temperature of 900 to 920^0C, the sample show a stabilize end

product for YBCO powder. Moreover, from 920 to 950 ^{0}C, the final product shows a stabilize growth of $YBa_2Cu_3O_7$ added with Al_2O_3 nanoparticles powder.

The recommendation for future research may be extent to the mechanical properties of the addition, where the Al_2O_3 nanoparticles is known as the harder material that will elastically interact with dislocations within the $YBa_2Cu_3O_7$ grains and consequently prevent the dislocation movements during indented or any testing. Besides, the uses of higher conductivity of metal element addition will extent the properties of the HTSC for better application. Furthermore, this research may be continued with the conductivity testing such as the four probe test and electrical resistance measurement and may be suggested to be further into the pinning centre properties through J_C by using Alternating Current Susceptometer (ACS).

REFERENCES

Alecu, G. (2004). Crystal Structures of Some High-Temperature Superconductors. *Romanian Reports in Physiscs*, Volume 56 (No. 3). 404-412.

Aparimita, A. (2011). Synthesis And Characterization Of YBCO/CNT Composite. National Institute Of Technology Rourkela.

Azambuja ,P., Junior ,P. R.,.Jurelo ,A. R,.Serbena ,F. C, Foerster C. E., and Costa R. M. (2008). Effects of Ag Addition on Some Physical Properties of Granular $YBa2Cu_3O_{7-\delta}$ Superconductor. *Brazilian Journal of Physics*, vol. 39(no. 4), 638-644.

Bagheri, M, M. M., Shahtahmasebia ,N., Alinejada M.R., Youssefic A., Shokooh-Saremi, M. (2008). The effect of the post-annealing temperature on the nano-structure and energy band gap of SnO2 semiconducting oxide nano-particles synthesized by polymerizing–complexing sol–el method". *Physica B* 403 , 2431–2437.

Benzia, P.b., Bottizzoa ,E., Rizzia ,N.(2004). Oxygen determination from cell dimensions in YBCO superconductors. *Journal of Crystal Growth* 269 (2004) 625–629, 1-5.

Bhadeshia, H.K.D.H., (2002). Thermal analyses techniques. Differential thermal analysis. University of Cambridge, *Material Science and Metallurgy.*(1-4)

Cyrot, M., Pavuna, D. (1992). Introduction to superconductivity and high-T_c materials. Singapore : Continental Press.

Devendra Kumar, N.; Raju ,M. S., P.; Naik ,P. K., S., Rajasekharan, T., Seshubai, V. (2013, February 28). Effect of Ag addition on the microstructures and superconducting. *Physica C*, 1-5.

Felt, U., Nowotny ,H. (1992). Striking Gold in the 1990s: The Discovery of High-Temperature Superconductivity and Its Impact on the Science System. *Science, Technology, & Human Values* 17,4, 506-531.

Ghosh, S.C., Thanachayanont, C. and Dutta, J. (2014) Studies on Zinc Sulphide Nanoparticles for Field Emission Devices. *The* 1*st ECTI Annual Conference* (*ECTI-CON*2004), Pattaya, 13-14 May 2004, 145-148.

Giri, R., Awana, V.P.S., Singh, H.K., Tiwari, R.S., Srivastava, O.N., Gupta, A.,Kumaraswamy, B.V., Kishan, H. (2005). Effect of Ca doping for Y on structural/microstructural and supercondivity properties of $YBa_2Cu_3O_7$, *Physica C : Superconductivity*, 419(3-4), 101-108.

Grant,P.M., Beyers, R.B, Engler E. M.,G. L, Parkin,S.S.P., Ramirez ,M.L. , Vazquez, J.E. (1987). Superconductivity above 90 K in the compound. *Phys. Rev. B*, Volume35 (issue 13), 7242-7244.

Hazen ,R. M., Finger, L. W., Angel, R. J., Prewitt ,C. T., Ross ,N. L., Mao ,H. K., Hadidiacos,C. G., Hor, P. H., Meng ,R. L., and Chu ,C. W. (1987). Crystallographic description of phases in the Y-Ba-Cu-O superconductor. *Phys. Rev. B 35*, Volume 35(Issue 13). 7238-7241.

Howe, B. A. (2014). Crystal Structure and Superconductivity of $YBa_2Cu_3O_{7-x}$. (Degree of Master of Science in Physics), Minnesota State University, Mankato Minnesota.1-59.

Jabbar,A.,.Qasim,I.,Mumtaz,M.,Nadeem ,K. (2014). Synthesis and superconductivity of (Ag)x/CuTl-1223 composites Materials Research Laboratory, Department of Physics, Faculty of Basic and Applied Sciences (FBAS), Internationa Islamic University (IIU), Islamabad 44000, Pakistan Progress in Natural Science: *Materials International 25*, 204-208.

Khoshnevisan, B. (2002) .Diffraction studies of the structural phase transition in the High Temperature Superconductor YBCO, Neutron Scattering and Material Physics Group, Joule physics laboratory, Institute for Materials Research, University of Salford.

Kumar, P.,Pillai, V., Shah, D. O. (1993). Preparation of $YBa_2Cu_3O_{7-x}$ superconductor by oxalate coprecipitate, *Journal of material science* ,12, 162-164.

Larimi, Z.M., Amirabadizadeh, A., Zelati, A. (2011).Synthesis of Y_2O_3 Nanoparticles by Modified Transient Morphology Method, International Conference on Chemistry and Chemical Process IPCBEE, IACSIT Press, Singapore, vol.10, 86-90.

Lundy ,D. R., Swartzendruber ,L. J., and Bennett ,L. H., (1989). A Brief Review of Recent Superconductivity Research at NIST. Number 3 *Journal of Research of the National Institute of Standards and Technology*, Volume 94, 147-155.

Li, S., Sellers, M. S., Basaran, C., Schultz, A. J., & Kofke, D. A. (2009). Lattice Strain Due to an Atomic Vacancy. *International Journal of Molecular Sciences*, *10*(6), 2798–2808.

Liu, Y. and Yang, Y.P. (2015). Evolution of the Surface Area of Limestone during Calcination and Sintering. *Journal of Power and Energy Engineering, Volume 3,* 56-62.

Lleonart, J. A. (2014). Study of the Resistive Switching phenomenon in YBCO. *Nanoscience and Nanotechnology*, 1-26.

Mellekh, A., Zouaoui, A., Ben Azzouz, E., Annabi, A. and Ben Salem, A. (2006). Nano-Al_2O_3 particle addition effects on YBa2Cu3Oy superconducting properties. *Solid State Communications*, Volume 140, 6 , 318-323.

Menad ,D. N.(2011). High Temperature Materials; Sintering and Consolidation of Ceramics Department of Chemical Engineering and Geosciences, Division of process metallurgy, Lulea University of Technology(Sweden).

Moulson, A.J, Herbert. J. M. (2003). Electroceramic. Chichester,West Sussex, England: John Wley & Sons Inc. ISBN 0471497487.

Mourachkine, A. (2002). High Temperature Superconductivity in Culprates.United State : Kluwer Academic pulisher.

Marouchkine, A., (2004) . Room - Temperature Superconductivity .*Cambridge International Science Publishing* .ISBN 1-904602-27-4

Nenartaviciene, G., Tonsuaadu, K., Jasaitis, D., Beganskiene, A., Kareiva, A. (2007). Preparation and characterization of superconducting $YBa_2(Cu_{1-x}Cr_x)_4O_8$ oxides by thermal analysis. *Journal of Thermal Analysis and Calorimetry* 90: 173 –178.

Olevsky ,E. A., (2011).Sintering Theory Brief Introduction, San Diego State University, California, USA.

Parida, B. ,(2011) DC Electrical Resistivity Studies In Bulk YBCO/Ag Composites. (M.Sc Physics), National Institute Of Technology, Rourkela.

Rajan, T.V., Sharma, C.P., Sharma, A.(2011). Heat Treatment Principle and Techniques. New Dehli: PHI learning Private limited.

Rani, P., Jha ,R. and Awana ,V.P.S. AC susceptibility study of superconducting $YBa_2Cu_3O_7$:Agx bulk composites (x = 0.0-0.20): The role of intra and inter granular coupling. *Quantum Phenomena and Application*.1-15.

Rose-Innes, A.C., Rhoderick, E.H. (1978). Introduction to superconductivity. (2^{nd} ed.). New York : Pergamon press.

Sadhana, B.,Bansal, T.K., Mcgreevy, R.L., Smith, S.H., Guarton, G. (1988). Effect of heat treatments on Y-B-Cu-O and Y-Gd-Ba-Cu-O superconductors. *Mat. Res. Bull*.,23,843-850.

Sahoo,M.,Behera,D.(2012).Study of $YBa_2Cu_3O_{7-\delta}/Al_2O_3$ Composite for Structural and Electrical Transport Property. *International Journal of Scientific and Research*, Volume 2(issue 9).1-6.

Salamati, H., Brojeny ,A. A. B. and Safa, M. (2001). Investigation of weak links and the role of silver addition on YBCO superconductors. *Superconductor Science and Technology*, Volume 14 (Number 10).

Safranski,C. (2010). Resistance of the Superconducting Material YBCO. (the Degree Physics BS), California Polytechnic State University, San Luis Obispo.1-44.

Schubert, U., Husing, N., (2005) Synthesis of Inorganic Materials, *"Wiley-VCH, Weinheim*, SSBN 3-527-31037-1.

Schilling, A., Cantoni, M., Guo, J. D. and Ott, H. R. Superconductivity above 130-k in the Hg-Ba-Ca-Cu-O system. Nature. (1993). Vol. 363. No. 6424. 56-58.

Sheahen, Thomas, P. (2004). Introduction to High-Temperature Superconductivity. Edited by Stuart Wolf. New York, New York: Springer-Verlag.

Singh, K.A., Pathak, L.C., Roy, S.K. (2007). Effect of citric acid on the synthesis of nanocrystalline yttria stabilized zirconia powders by nitrate–citrate process, Ceram. Int. 33 , 1463–1468.

Suan, M. S. M., Johan. M. R. (2014). Microhardness of Al_2O_3 nanoparticles added $YBa_2Cu_3O_{7-\delta}$ Superconductor Prepared Using Auto-combustion Reaction, *Materials Research Innovations*, VOL 18 ,66-73.

Suan, M.S.M., Johan , M.R. (2013) .Synthesis of Al_2O_3 nanoparticles highly distributed in $YBa_2Cu_3O_7$ superconductor by citrate–nitrate auto-combustion reaction. *Physica C* 492 , 49-54.

Sukirman, E., Winatapura, D.S, Adi, W.A.,Yustinus, P.(2007). The Influence of Lattice Strain to the Critical Current Density of YBCO. *Indonesia Journal of Material Science*, 46-52.

Sukirman, E., Wisnu AA, Yustinus P, Sahidin W, D., & Rina M, Th. (2009). Synthesis and Characterization of Nano Scale YBCO. In Toto Hardianto (Ed.). *The Proceeding on National Seminar in Nuclear Science and Technology*, (p. 386). Indonesia: National Nuclear Energy Agency.

Syukor, R.A. (2009). High temperature superconductors : material, mechanisms and application. ASM Inaugral Lecture.

Tahirbegi, B. (2014). A New Approach to Size Dependent Breakdown of Superconductivity in Ultranarrow Nanowires. *American Journal of Condensed Matter Physics, 4*(2), 32-35.

Thakur,R.,Chawla ,P.(2015). High Temperature Superconducting Techniques and its Applications. *International Journal of Engineering Technology*, Volume 3 (Issue 5). 285-294.

Vinila, V.S., Jacob, R., Mony, A., Nair, H.G., Issac, S., Rajan, S., Nair, A.S., Satheesh, D.J. and Isac, J. (2014) Ceramic Nanocrystalline Superconductor Gadolinium Barium Copper Oxide (GdBaCuO) at Different Treating Temperatures. *Journal of Crystallization Process and Technology*, 4, 168-178.

West, A.R. (1974) Solid State Chemistry and It's Applications. Wiley, New York.

Widad M.,Faisal, Salwan ,K. J., Ani ,A. (2013). The influence of aluminum doping and oxygenation on the properties of YBa_2Cu_3-x$Al_xO_{6.5+\delta}$ ($0 \leq x \geq 0.045$) HTSC. *Int. J. Nanoelectronics and Materials ,6*, 1-4.

Zhang,C.,Kulpa,A.,A.C.D.Chaklader.(1995).Silver solubility in $YBa_2Cu_30_x$. *Physica C 252*, 67-78.

APPENDIX

The calculation for $YBa_2Cu_3O_7$ Preparation :

From this synthesis, the 5g of pure $YBa_2Cu_3O_7$ was divided into five pellets that will have 1g for each sample.

$\frac{1}{2}Y_2O_3$	=	112.904 g/mol
$2BaCO_3$	=	394.674 g/mol
$3CuO$	=	238.635 g/mol
Total	=	746.215 g/mol

In preparing 5 g of sample, each of the components should weight :

$$Y_2O_3 = \frac{5(112.904)}{746.215} = 0.757 \text{ g}$$

$$BaCO_3 = \frac{5(394.676)}{746.215} = 2.645 \text{ g}$$

$$CuO = \frac{5(238.635)}{746.215} = 1.599 \text{ g}$$

$$\text{Total} = 4.986 \text{ g} \approx 5 \text{ g}$$